

Design and Implementation of Z-Source Inverter by Simple Boost Control Technique for Laboratory Scale Micro-Hydropower Application

Rizki Mendung Ariefianto^{1*}, Rizky Ajie Aprilianto², Heri Suryoatmojo³, and Suwito³

¹*Department of Electrical Engineering, Universitas Brawijaya*

Jl. Veteran, Ketawanggede, Lowokwaru District, Malang City, East Java, 65145, Indonesia

²*Department of Electrical Engineering and Information Technology, Universitas Gadjah Mada
Bulaksumur, Caturtunggal, Depok District, Sleman Regency, Special Region of Yogyakarta, 55281, Indonesia*

³*Department of Electrical Engineering, Institut Teknologi Sepuluh Nopember
ITS Campus, Keputih, Sukolilo District, Surabaya City, East Java, 60111, Indonesia*

*Corresponding author. Email: rizkimsahab19@gmail.com

Abstract— In a power plant such as micro-hydropower (MHP), an induction generator (IG) is usually employed to produce electrical power. Therefore, an inverter is needed to deliver it with high efficiency. Z-source inverter (ZSI) has been introduced as a topology with many advantages over conventional inverters. This research aims to investigate the performance of ZSI based simple boost control (SBC) in laboratory-scale MHP systems using a rewinding induction generator. This research has been conducted both from simulations and experiments. Based on the result, the waveform characteristic and value of ZSI are close to the desired design. A shoot-through duty ratio of 17% can reach 60 Vrms output voltage, and this condition has a conversion ratio of about 2.05 times. Also, SBC can significantly reduce the Total Harmonic Distortion (THD). ZSI efficiency has a value of 84.78% at 50% of rating load 100 W and an average value of 80%. Compared to the previous study, the proposed design has more economical with the same component for the higher rating power. Moreover, it has a smoother and entire output waveform of the voltage.

Keywords— micro-hydropower, induction generator, simple boost control, z-source inverter

I. INTRODUCTION

Electricity generation based on fossil energy alone is appraised as inadequate for the growth of demand energy capacity. Besides, the utilization of fossil energy adversely affects the increase of environmental pollution and the greenhouse effect. This problem encourages many researchers to utilize renewable energy resources more and promote non-emission electricity for better human social development. [1], [2]. Some renewable energy such as solar energy, geothermal, wind energy, biomass, and hydro become options to generate electricity from sustainable energy in the future [3]. Among all renewable energy resources, micro-hydropower (MHP) is considered the most favorable energy source, which has an efficient, clean, and uncomplicated technology [4]. Hence, this power generation technology deserves to implement in remote areas with intricate geographical contours, such as mountainous areas.

The utilization of renewable energy can be installed either standalone or grid system [5]. The MHP system implemented in an isolated area is possible for a standalone system. This concept used in specific locales is mostly not connected to the grid. Standalone systems of MHP constitute renewable solutions that can give a low-cost power supply with more good social and environmental sustainability than a grid-connected system [6]. The MHP system generally utilizes an induction generator (IG) to convert mechanical energy into electricity. It is selected

because of some merits such as costless, reliable, simple operation, brushless, without DC excitation, and a long lifetime without any severe problem [7].

After the electrical power has been converted, the IG requires an electrical circuit to deliver the load power optimally. Therefore, the use of electrical circuits with high efficiency is essential. One of the most important electrical devices is an inverter, which the popular technology is Voltage Source Inverter (VSI) and Current Source Inverter (CSI) [8]. The other inverter topology is introduced that is familiar enough for renewable energy application. This topology is known as Z-source Inverter (ZSI), which was investigated in [9] - [11]. ZSI has a unique circuit because it consists of two identical inductors and capacitors crossing each other, utilizes the shoot-through state to increase performance, and operates as a voltage/current source type of inverter [12].

Moreover, ZSI can also operate either buck mode or boost mode, which is more beneficial to overcome the drawbacks of two-stage configurations [13]. The other advantage of ZSI is no need for time delay regulation [14], able to avert the output waveform from the distortion [15], vast voltage operation [16], and adding a shoot-through to avoid inverter short circuit [17]. Consequently, it can boost the input voltage with good output voltage quality [18].

Many researchers have been testing ZSI on renewable energy applications. In [19], ZSI is applied for the MHP emulator using standard PWM switching. The ZSI maximum

efficiency is obtained around 80% and is almost constant for wide-range power. In [20], ZSI has been implemented in photovoltaic applications with the result that this topology is more appropriate for both standalone and grid applications. The comparison between ZSI and other topologies for small wind turbines has been investigated [21]. It has good reliability for the conversion systems and reduces the voltage stresses. Another comparison between ZSI and conventional inverter topology has been presented in [22]. This comparison is applied in a fuel cell with the result that ZSI gives a more suitable DC-link voltage.

For ZSI applications, most studies focus on conventional switching with simulation schemes. Therefore, experimental validation is required to confirm the performance result of the simulation. Different strategy control is needed to improve the performance of ZSI. One of the best strategies for ZSI topology is simple boost control (SBC). This strategy has some advantages, such as being easy to control [23] and having good characteristics [24]. The merit of SBC is also emphasized in [25], wherein this strategy can reduce the harmonic output properly and increase the power density. Hence, it is suitable for grid power quality improvement.

This paper aims to design and implement a ZSI topology controlled by a simple boost strategy. The simulation and experimental investigation were carried out to confirm its performance. Furthermore, the experimental design of ZSI is applied to a micro-hydropower for laboratory-scale based on induction generators to validate the simulation result. The application of ZSI in MHP with a standalone system is predicted to increase the inverter roughness and maintain the characteristics of the turbine in a suitable condition.

II. METHOD

Figure 1 shows the proposed configuration design system. The systems consist of an induction generator rotated by a prime mover to produce AC voltage. Then a 3-phase rectifier device converts it into DC voltage. A bank capacitor is utilized to supply field current on the induction generator. The output voltage has functioned as input of ZSI that consists of two identical inductors and capacitors connected to the 3-phase inverter. An LC filter installs on the output side to produce pure sinusoidal voltage. The 3-phase inverter switching uses simple boost control to maintain the constant output voltage with shoot-through duty ratio adjustment.

ZSI topology depicted in Figure 2 only uses two identical inductors and capacitors crossing each other to produce the desired voltage [12]. In ZSI impedance, the inductor components work to reduce current ripples, while the capacitor component is used to compensate for these ripples to keep the constant output voltage [10]. ZSI can overcome the drawback of conventional inverters such as VSI and CSI. The conventional inverter cannot operate on both modes, as step-up and step-down. Meanwhile, ZSI can increase input voltage (boost mode) and otherwise (buck mode) without auxiliary switching. The total switching on ZSI is written in (1).

$$T = T_0 + T_1 \tag{1}$$

where T_0 is a shoot-through period and T_1 is a non-shoot through period.

There are three operating modes on ZSI: active conditions, null conditions, and shoot-through zero states. An analysis is carried out by assuming the ideal component. The theoretical waveforms are shown in Figure 3. In shoot-through zero states

or during the T_0 period, the inductor current will increase, the capacitor in discharge mode, and the voltage across the inductor will appear. Meanwhile, in non-shoot through zero states or during the T_1 period, the inductor current will decrease, the capacitor in charge mode, and the inductor voltage will be zero.

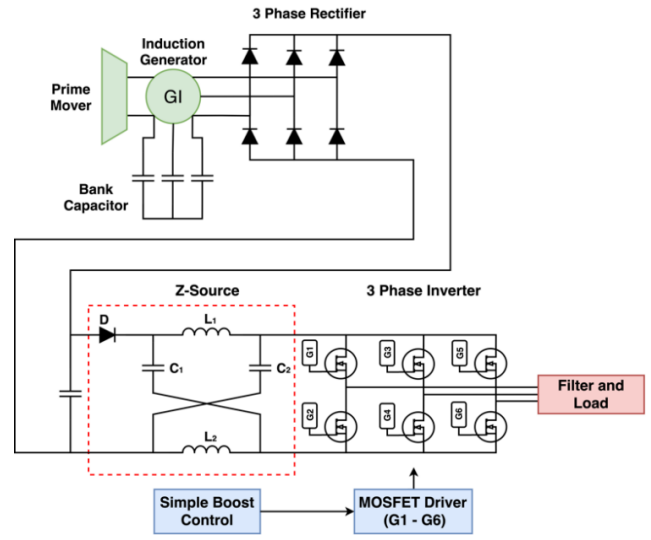


Figure 1. The proposed design systems

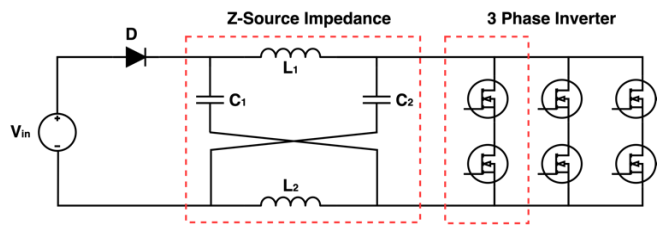


Figure 2. Z-source Inverter topology

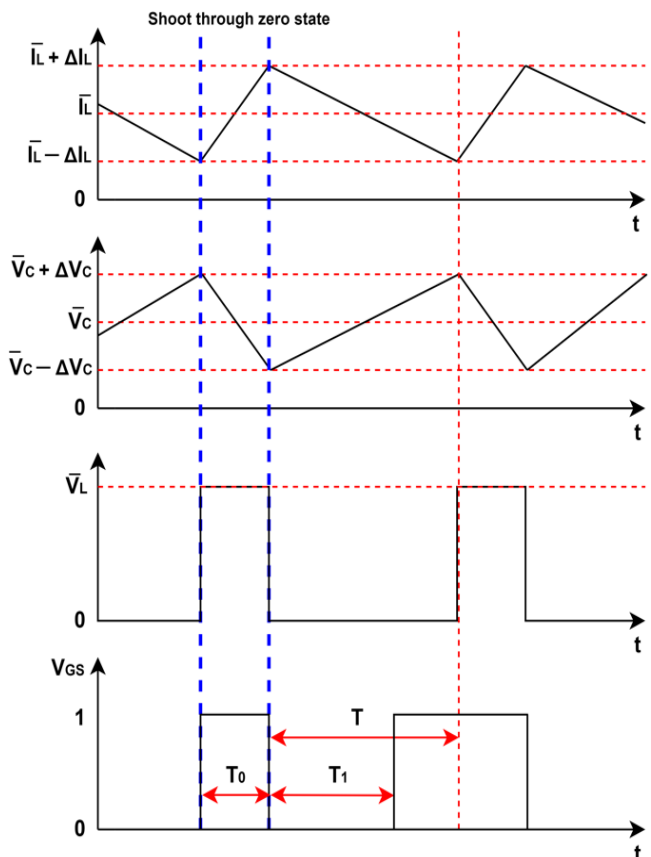


Figure 3. The theoretical waveforms of ZSI

1) Mode I (Active Condition)

In this circumstance, the DC source is charged to the ZSI circuit that consists of two identical inductors and capacitors. The capacitor is charged, and the energy will flow to the load through the inductor component. Based on the condition, the inductor suffers discharging. The equivalent circuit of ZSI on mode I is shown in Figure 4(a).

2) Mode II (Null Condition)

ZSI operates in one of two null conditions. DC voltage flows to the inductor and capacitor. The switch suffers a short circuit either on the bottom or top. As long as this mode, the inverter bridge becomes an open circuit condition because the current flows to the load equivalent reach zero value ($I_x = 0$). Figure 4(b) shows the equivalent circuit on this mode.

3) Mode III (Shoot-Through Zero States Condition)

ZSI operates on one of seven shoot-through zero states conditions. The inverter bridge circuit suffers short circuit again, resulting in zero output voltage on the inverter bridge. The capacitor voltage will gradually boost related to the shoot-through duty ratio. Figure 4(c) shows the equivalent circuit on mode III.

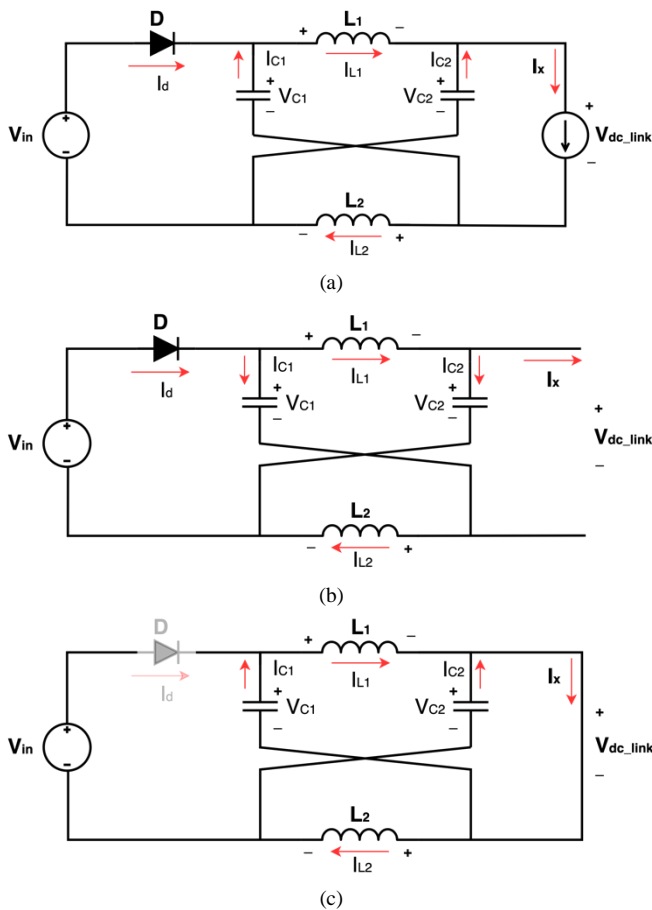


Figure 4. ZSI on (a) active condition, (b) null condition, and (c) shoot-through zero states

On the ZSI topology, the DC-link voltage is written in (2), while the boosting factor (B) is given in (3).

$$V_{dc-link} = BV_{rec} \quad (2)$$

$$B = \frac{1}{1 - \left(\frac{2T_0}{T_1}\right)} \quad (3)$$

V_{rec} is the rectifier output voltage as ZSI input. Then, equation (4) gives the peak output phase voltage as follows:

$$\hat{V}_{ac} = MB \frac{V_{rec}}{2} \quad (4)$$

M is the modulation index with a value of $M \leq 1$. At the time of shoot-through condition with a period of T_0 , it can be found that the shoot-through duty ratio has a value, which is expressed in (5).

$$\frac{T_0}{T_1} = \frac{B - 1}{2B} = D_0 \quad (5)$$

If T is the switching period, then the switching frequency (f_s) is $1/T$. Hence, D_0 can satisfy the formula in (6).

$$D_0 = T_0 f_s \quad (6)$$

During the non-shoot through time, the inductor current decreases linearly, and its voltage is different from the input and capacitor voltage. The average inductor current is formulated in (7).

$$\bar{I}_L = \frac{P}{V_{rec}} \quad (7)$$

The maximum current ripple that passes through the inductor occurs when the shoot-through is maximum, so the peak to peak current ripple (ΔI_L) on the inductor needs to be determined by maximum and minimum inductor current, which is calculated by (8) and (9), respectively. As a result, ΔI_L can be found in (10).

$$I_{Lmax} = \bar{I}_L + (0.5\bar{I}_L \times \%ripple) \quad (8)$$

$$I_{Lmin} = \bar{I}_L - (0.5\bar{I}_L \times \%ripple) \quad (9)$$

$$\Delta I_L = 2(I_{Lmax} - I_{Lmin}) \quad (10)$$

During the shoot-through zero states mode, the value of $V_L = V_C = V$. The value of V can be expressed in (11).

$$V = \frac{(B + 1)}{2} V_{rec} = \frac{1 - D_0}{1 - 2D_0} V_{rec} \quad (11)$$

so that the inductor and capacitor value is formulated in (12) and (13) respectively [13].

$$L = \frac{VT_0}{\Delta I_L} \quad (12)$$

$$C = \frac{\bar{I}_L T_0}{V \Delta V_C} \quad (13)$$

The filter that used in ZSI circuit can be determined in (14) for inductor and (15) for capacitor.

$$L_f \geq \frac{D_0 R_L}{2f_s} \quad (14)$$

$$C_f = \frac{1}{0.03 \times V_{rec} \times V_{dc-link} \times f_s} \quad (15)$$

where R_L is load resistance.

SBC can regulate the output voltage by adding shoot-through zero states for each switches component [26]. Two DC signals employ the shoot-through duty ratio (D_0). The first signal is equal to the peak value of the three-phase reference signal, while the second signal is the negative value of the first signal. When the triangular carrier signal is higher than the positive DC signal (V_{PO}) or less than the lower limit DC signal (V_{NE}), the circuit will be in a shoot-through state [27]. Finally, the process above will generate the gate driving signal, which has characteristics in Figure 5.

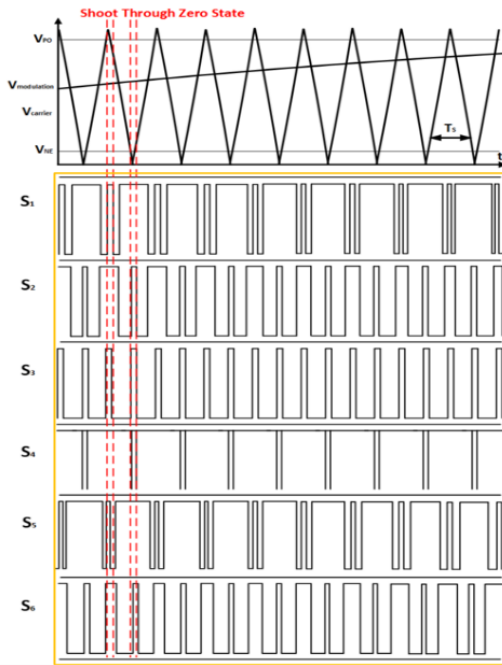


Figure 5. Simple boost control signal

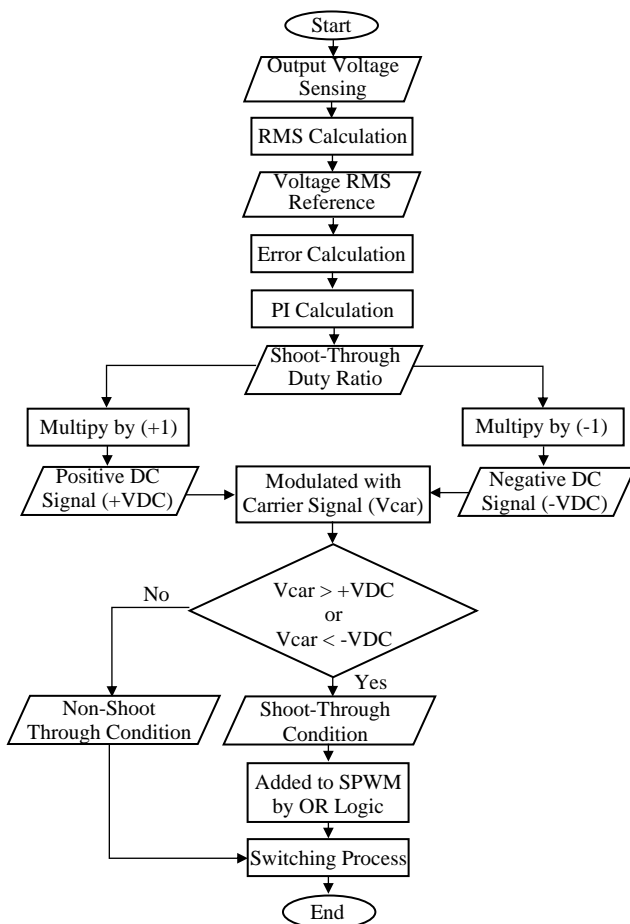


Figure 6. Flowchart of voltage control using SBC

As shown in Figure 6, to obtain the output of the SBC system, the load voltage is read by the voltage sensor and converted to the RMS value. Next, it is compared with the reference voltage to result in the error value as an input of the PI controller. The PI controller generates the shoot-through duty ratio (D_0). To produce a shoot-through signal, the value of D_0 is multiplied by 1 and -1 to produce the required DC

voltage on the SBC. The switching characteristics of the MOSFET inverter are highly dependent on the results of the comparison between the DC voltage and the carrier signal to produce shoot-through conditions. When the carrier signal is higher than the positive DC signal or less than the lower limit DC signal, the circuit will be in a shoot-through state. Outside of both conditions, it becomes a non-shoot-through state. Then, a shoot-through condition is added to the SPWM circuit for switching in all MOSFETs whose mechanism is regulated using OR logic gates. Three conditions worked in the switching process: active, null, and shoot-through zero state conditions.

The experiment of ZSI using simple boost control for laboratory-scale MHP was carried out by supplying IG rotation using a prime mover. A variable frequency drive (VFD) controls the prime mover to obtain the desired rotation. It is necessary to rotate IG above a synchronous speed of about 1490 rpm based on its rating. Moreover, the capacitor bank of 257 μF is used to generate the field current of IG. Figure 7 shows the complete setup of IG as the input of ZSI.

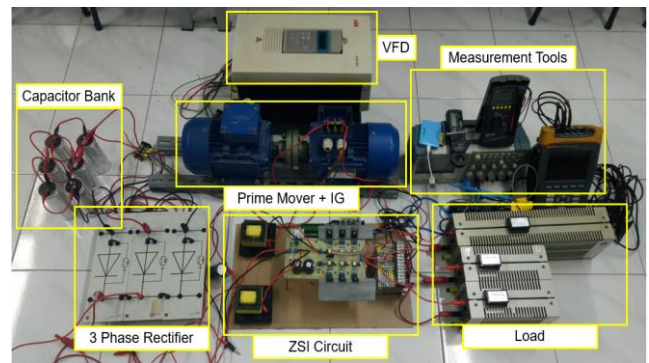


Figure 7. Hardware experimental set-up

This configuration can ensure the production of an input voltage for the ZSI circuit. The IG used is a rewinding machine, so it has a rated phase voltage of 56 V, as shown in Table I. The ZSI circuit is designed with the initial parameters shown in Table II. Then, Table III summarizes ZSI impedance, simple boost control, and driver components. The simulation design of ZSI using the SBC technique is conducted in PSIM software, as shown in Figures 8(a) and 8(b), respectively. Then, Figure 9 shows the experimental setup of the ZSI device.

TABLE I. INDUCTION GENERATOR SPECIFICATION

No	Parameter	Value/Type
1	Rotor Type & Power	Squirrel cage
2	Output Power	1 HP
3	Rated Phase Voltage	56 V
4	Frequency	50 Hz
5	Pole number (p)	4
6	Rated Speed (n)	1390 rpm
7	Efficiency (η)	73%
8	Bank Capacitor	257 μF
9	Rectifier	Three phases
10	Filter Capacitor	850 μF

TABLE II. INITIAL SPECIFICATION OF ZSI

No	Parameter	Description	Value
1	P	Rated Power	100 W
2	V_{rec}	Input Voltage	52 V
3	V_p	Peak Output Voltage	35 V
4	V_{rms}	Line to Line Voltage	60 V
5	M	Modulation Index	0.92
6	f_s	Switching Frequency	7.842 kHz

TABEL III. COMPONENT IMPLEMENTATION OF ZSI AND SBC

Sub Device	Parameter	Value / Type
ZSI	Inductor (L_1 and L_2)	8.25 mH
	Capacitor (C_1 and C_2)	470 μ F
	Diodes	MUR1560
	MOSFET 1 – 6	IRFP460
	LC output filter	$L = 10$ mH, $C = 6$ μ F
	SBC	Microcontroller
	IC Logic	HD74HC04P
	IC Not Logic	SN74LS32N
	Gate Driver	FOD3182V

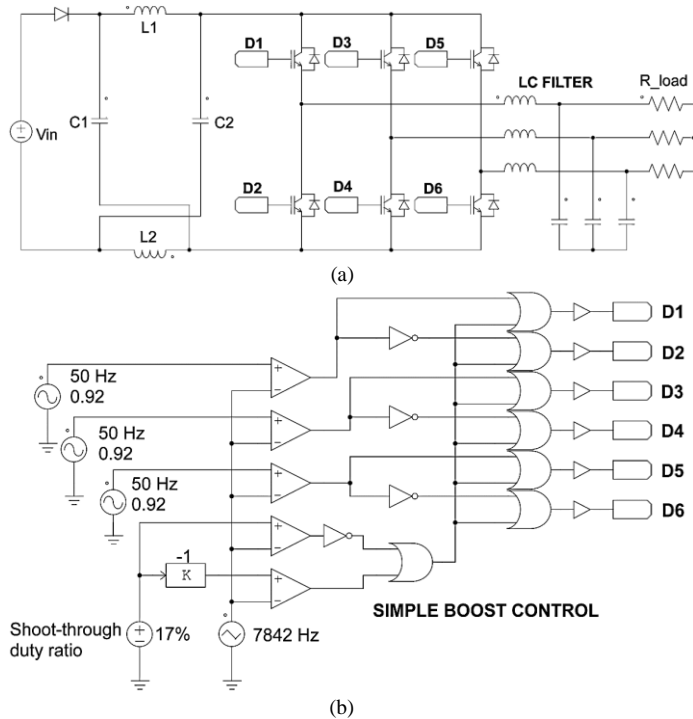


Figure 8. Design of simulation PSIM: (a) ZSI circuit and (b) SBC circuit

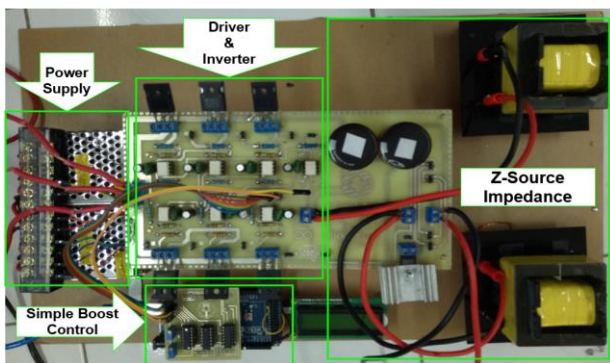


Figure 9. ZSI implementation using SBC strategy

III. RESULTS AND DISCUSSION

A. Testing of Rewinding Induction Generator Output

Induction generator testing aims to determine the output voltage produced by an induction motor when operated as a generator. The rewinding induction generator was applied in this campaign. Hence, this machine has an RMS voltage of 56 V in normal operation. As a generator, the induction motor must be rotated above its synchronous speed and installed a capacitor bank as a reactive power supplier. The rating speed of the induction machine is 1390 rpm, so in this test, 1492 rpm speed is applied. From this test, the AC output voltage is about 45 V RMS which means below the machine voltage rating as

shown in Figure 10(a). Furthermore, this voltage is rectified by a 3-phase rectifier and smoothed by a filter capacitor to obtain the DC voltage around 52 V as the voltage input of ZSI. Figure 10(b) shows the DC voltage characteristic of this experiment.

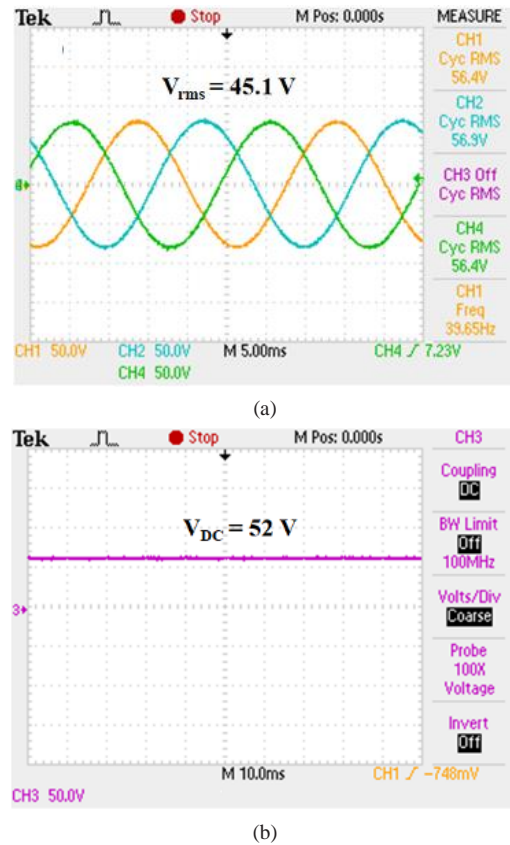


Figure 10. Voltage waveform of induction generator: (a) before rectified and (b) after rectified

B. Testing of Simple Boost Control

The test is conducted by analyzing a simple boost control waveform with a switching frequency input of 7.842 kHz. Based on the test results, the switching period is 128 μ s, so the switching frequency is around 7.8 kHz. This frequency is also close to the desired value from the simulation, which is 7.842 kHz or comparable to 127.5 μ s. Figure 11 shows the characteristics of a simple boost control waveform.

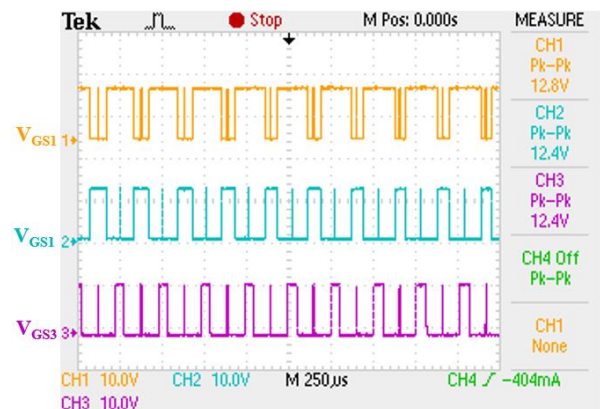


Figure 11. Simple boost control waveform

C. Testing of ZSI Waveform

Figure 12 shows the comparison between the capacitor and inductor voltage waveforms. When the switch is in non-shoot-through zero states, capacitors C_1 and C_2 are charging and have zero inductor voltage. Meanwhile, when the switch is in shoot-

through zero states, the capacitors C_1 and C_2 discharge, and a voltage will appear on the inductor. Hence, this condition leads to the inductor voltage is similar to the capacitor voltage. The magnitude of the voltage across the inductor and the capacitor has the same value of about 72 V, which is close to the calculation result of 65.4 V, simulation 65.5 V. Based on the relation, $V_{dc_link} = 2V_C - V_{in}$, it can be determined the peak value of the DC-link voltage about of 78.8 V and 79.1 V for calculation and simulation, respectively.

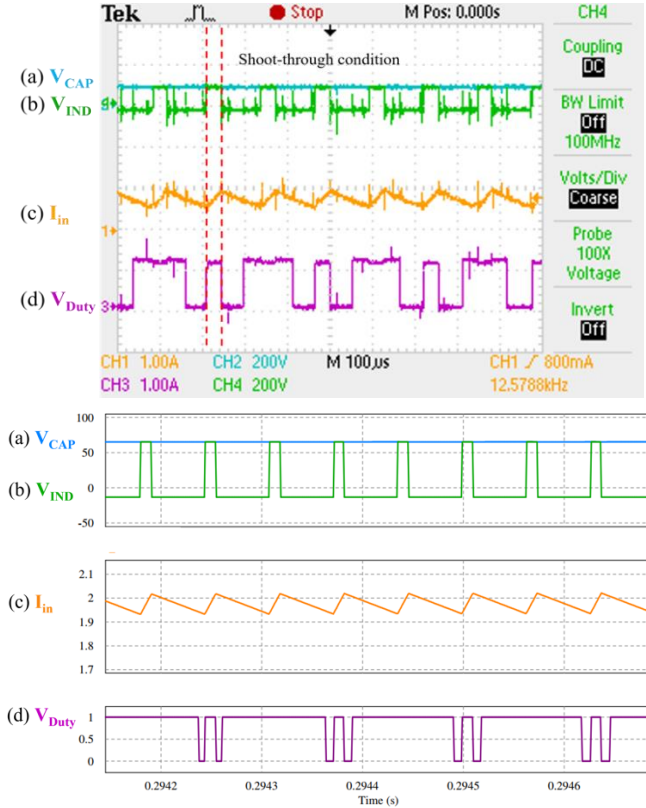


Figure 12. ZSI waveform implementation (above) and simulation (below) (Note: (a) capacitor voltage, (b) inductor voltage, (c) inductor current, and (d) gate source waveform)

In Figure 13, the peak DC-link voltage of the experiment reaches up to 88 V. The DC-link voltage has zero value at shoot-through condition, which means the inverter leg is in a short circuit. There is non-linear relation between the peak of DC-link and capacitor voltage, but it can be regulated using capacitor voltage control as proposed in [28]. This experiment did not insert the DC-link capacitor to make the distortion of DC-link voltage. Hence, the inverter side is not supplied by pulsed currents. Consequently, it distorts the input source due to the reflect phenomena. Moreover, super-imposed spikes and noises in the DC-link voltage of ZSI are caused by semiconductor switching and massive inrush current due to the shoot-through condition [29]. In addition, the inductor current increase during shoot-through condition with an average value is 2.1 A in this experiment, which is slightly different from its design current of 1.92 A. Briefly, the value in the experiment is higher than both calculations and simulation process.

D. Testing of ZSI Output Voltage and Current

When ZSI is loaded by 120 Ω, ZSI can keep the voltage constant at 60 Vrms and the current of 0.239 A, respectively.

Both variables produced a period of about 20 ms that means they can form 50 Hz frequency in the load side. Figures 14(a) and 14(b) show the output voltage and current waveforms, respectively.

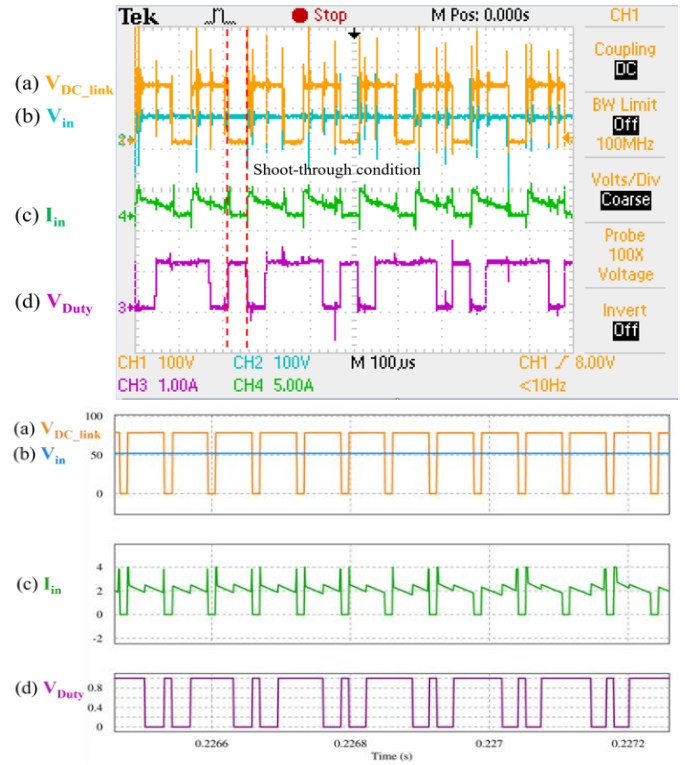


Figure 13. ZSI waveform implementation (above) and simulation (below) (Note: (a) DC-link voltage, (b) input voltage, (c) input current, and (d) gate source waveform)

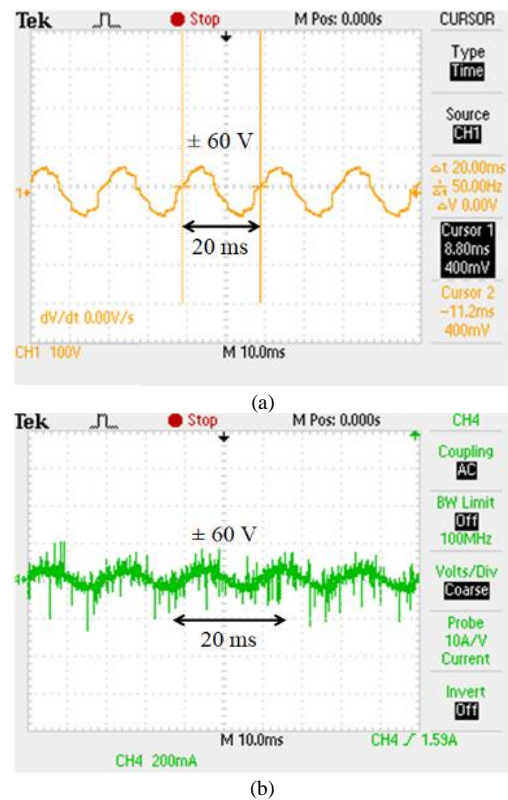


Figure 14. ZSI output waveform characteristic: (a) voltage and (b) current

The resulting waveform by ZSI is also 120° apart, proving that it produces a three-phase waveform as described in Figure 15. A passive filter on the output side can produce the sine waveform. The total harmonic distortion (THD) at the output voltage is also analyzed, as shown in Figure 16. An enormous RMS voltage value is found at the fundamental frequency of 50 Hz, while the other RMS voltage values are spread over the n -th order frequency. The THD value of the output voltage waveform is 7.43%. This value is relatively low, so it can be concluded that the simple boost control technique works appropriately to reduce the harmonic output. However, the THD value still must be minimized more until the requirement of standard THD is below 5%.

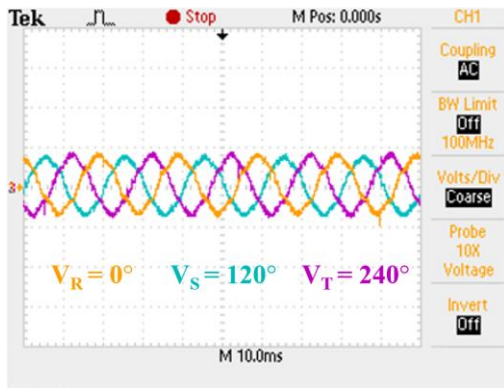


Figure 15. Three phase waveforms in ZSI output side

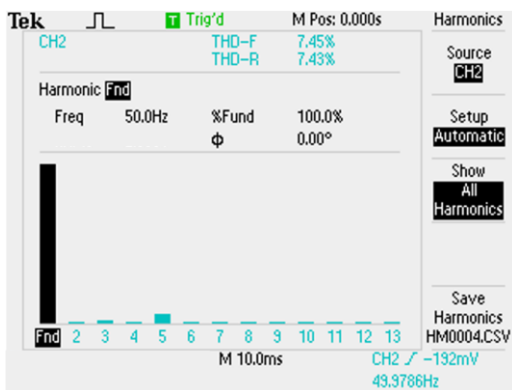


Figure 16. Total harmonic distortion of output voltage

E. Testing of ZSI Conversion Ratio

The conversion ratio test aims to determine the voltage increase factor in the ZSI circuit. The conversion ratio test is conducted by supplying a constant input voltage of $V_{in} = 52$ V, and the shoot-through duty ratio is increased gradually in the range of 0 – 20%, with the final voltage output target is 60 V. The higher shoot-through duty ratio, the larger output voltage that will be obtained. Based on the test, the final output voltage is reached in a shoot-through duty ratio of 17%, slightly different from the simulation test as shown in Figure 17. The conversion ratio at this shoot-through duty ratio is about 2.05 times.

F. Testing of ZSI Efficiency

The efficiency testing is carried out to determine the effect of inverter performance. In this test, the efficiency is determined by comparing the input power with the inverter output power. Inverter efficiency testing increases the shoot-through duty ratio at a different load. Figure 18 shows the ZSI efficiency from the experiment, with an average efficiency of

80%. ZSI has the highest efficiency of 84.78% at 50 W (50% of rating load) and has the lowest efficiency of 75.14% at 13 W (13% of rating load). In general, the load addition causes the accession of ZSI efficiency until a specific load, then decreases until full load. The losses factor causes this condition due to the voltage drop for shoot-through duty ratio addition. Voltage drops that occur in ZSI are caused by a non-ideal factor on inductors, capacitors, and semiconductor components [30]. In addition, the voltage drops also occur due to the switching losses, core inductor losses, fast switching diode loss, and charge-discharge capacitor loss.

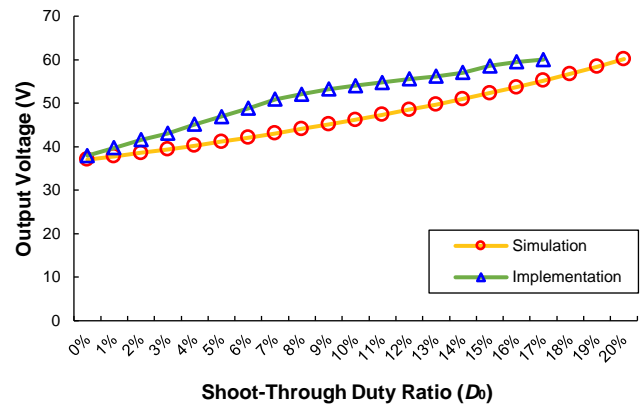


Figure 17. The comparison of ZSI conversion ratio

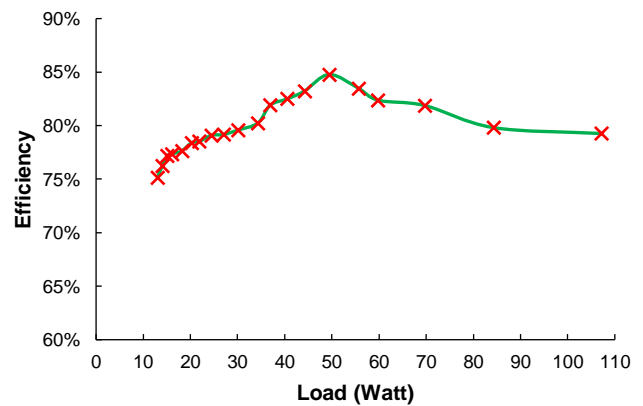


Figure 18. ZSI efficiency

In [31] explained that the efficiency of ZSI experienced a massive drop at low loads. Moreover, by increasing voltage gain, the efficiency tends to decrease. The two previous problem makes the large power circulation in the ZSI topology. The current flow becomes more extensive, increasing the power losses in the inductor, capacitor, and diode components. Figure 18 shows that the efficiency drop occurs before reaching the rating load. This characteristic is appropriate to [31], wherein the highest efficiency is achieved before nominal loads.

Based on [32], the SBC method has a maximum shoot-through duty ratio of $1 - M$, which means only 8% of the modulation index of 0.92. Meanwhile, the shoot-through design of ZSI in this experiment is 17%. Hence, it is clear that the shoot-through value used is higher than the allowable operating value on the SBC. This condition possible to make a higher shoot-through value and affects the efficiency decrease. Therefore, designing ZSI using SBC should consider the shoot-through limits allowed on SBC and choose the appropriate modulation index.

G. Result Comparison

Compared to the VSI and CSI topology connected to the buck or boost converter, ZSI can increase and decrease voltage only on a single circuit. In addition, ZSI only has one stage of power conversion, no need for dead time control, and is more economical because it uses fewer switching devices, as shown in Table IV.

TABEL IV. COMPARASION BETWEEN CONVENTIONAL INVERTER TOPOLOGY AND ZSI

Topology	The Number Switching Device	Conversation Stage	Dead Time Control
Buck-Boost with Conventional Inverter	7	2 stages	Yes
Z-Source Inverter	6	1 stage	No

Compared to similar experiments on ZSI, in [33] designed a ZSI with conventional PWM for a 6 W power rating that used the identical capacitor (C_1 and C_2) and inductor (L_1 and L_2) of 470 μ F and 10.1 mH, respectively. Using the same capacitor and 1.5 mH less of the inductor, ZSI with SBC in this study can apply on a rating of 100 W. Furthermore, in terms of the control mechanism, this study only used one microcontroller while [33] added another device that only functioned as a bridge between the main microcontroller and the voltage sensing. Hence, this results in higher experimental costs.

Table V shows several ZSI topologies with various switching methods. By employing the smaller shoot-through duty ratio in the comparable value of the modulation index, the ZSI with the SBC method can generate a boosting factor with a higher value. This result is more advantageous than the other method producing a boosting factor with a higher shoot-through duty ratio. For the THD aspect, ZSI based on SBC has an output voltage with THD of 3.16% and 7.43% in simulation and experiment, respectively. Surprisingly, simulation yields better THD than 7-levels ZSI controlled by maximum boost control (MBC), which has a THD of 10.13% [34].

The THD comparison of ZSI using SBC also yield a better result compared to ZSI using other methods such as Trapezoidal PWM (TPWM), Sinusoidal PWM (SPWM), and Space Vector PWM (SVPWM) [34]. Moreover, experimental research with similar consideration for line-to-line voltage of 60.78 V_{rms} and modulation index of 0.9 in [35] has THD value of 28.39% and 37.38% of both switching control applied. The output is obtained from an input voltage of 60 V_{dc}, which means the boosting factor is much smaller than ZSI using the SBC method.

TABEL V. COMPARISON OF ZSI WITH VARIOUS SWITCHING METHOD

No	Topology	M	B	D ₀ (%)	Voltage (V)		THD (%)	
					Input	Output	Simulation	Experimental
1	ZSI+SBC	0.92	2.05	17	52	60	3.16	7.43
2	7-level ZSI+MBC [34]	1.0	2.52	30	300	463	10.13	N/A
3	ZSI+CBPWM [35]	0.9	1.84	23	60	60.78	N/A	28.39
4	OD-ZSI [35]	0.9	1.84	23	60	60.78	N/A	37.38
5	ZSI+TPWM [36]	0.8	2.38	29	150	175	25.5	N/A
6	ZSI+SPWM [36]	0.8	2.38	29	150	175	10.60	N/A
7	ZSI+SVPWM [36]	0.8	2.38	29	150	175	4.17	N/A

The experimental result from [37] shows that the ZSI with SBC has an anomaly result because the output waveform of the voltage is distorted due to the auxiliary power supply. On the contrary, the present result with the same method yields a better result in which the output waveform of the voltage is smoother and undamaged. Hence, this study can rectify the voltage quality from the previous experimental study.

IV. CONCLUSION

This paper proposes a laboratory-scale MHP system with ZSI based on SBC. This research has been carried out both from simulations and experiments. A rewinding induction generator is used for this MHP system and functions as a ZSI voltage supply through a rectifier circuit. The waveform characteristic of ZSI is similar to the theoretical result, and its value is close to the desired design. The output voltage 60 V is reached in a shoot-through duty ratio of 17%, and this condition has a conversion ratio of about 2.05 times. SBC strategy can reduce harmonic output significantly until 7.43%. The efficiency of ZSI has a value of 84.78% at 50% of rating load 100 W and an average value of 80%. In general, the efficiency of ZSI rises with the increase in total load was given. Compared to the previous study, the existing experiment with the same method yields an economical design using the high rating power with the same component. Also, it has a smoother and undamaged output waveform of the voltage. This study is proven the limitation of ZSI design that should be considered. Next, changing the controller method and designing a filter with an appropriate value to reach THD less than 5% could be future research work.

ACKNOWLEDGMENT

The authors would like to thank gratefully for acknowledge financial support for this research by Institut Teknologi Sepuluh Nopember for the grants and Lembaga Pengelola Dana Pendidikan (LPDP).

REFERENCES

- [1] D. Gielen, F. Boshell, D. Saygin, M. D. Bazilian, N. Wagner, and R. Gorini, "The role of renewable energy in the global energy transformation," *Energy Strateg. Rev.*, vol. 24, pp. 38–50, 2019, doi: 10.1016/j.esr.2019.01.006.
- [2] R. M. Ariefianto, Y. S. Hadiwidodo, and S. Rahmawati, "Modelling of Unidirectional Oscillating Buoy Wave Energy Converter Based on Direct Mechanical Drive System under Irregular Wave," *IOP Conf. Ser. Earth Environ. Sci.*, vol. 698, no. 1, 2021, doi: 10.1088/1755-1315/698/1/012014.
- [3] W. I. Ibrahim, M. R. Mohamed, and R. M. T. R. Ismail, "Direct Power Control Method of Maximum Power Point Tracking (MPPT) Algorithm for Pico-Hydrokinetic River Energy Conversion System," *Lect. Notes Electr. Eng.*, vol. 632, pp. 691–703, 2020, doi: 10.1007/978-981-15-2317-5_58.
- [4] V. K. Singh and S. K. Singal, "Operation of hydro power plants-a review," *Renew. Sustain. Energy Rev.*, vol. 69, pp. 610–619, 2017, doi: 10.1016/j.rser.2016.11.169.

- [5] R. A. Aprilianto, Subiyanto, and T. Sutikno, "Modified SEPIC converter performance for grid-connected PV systems under various conditions," *Telkonnika (Telecommunication Comput. Electron. Control.*, vol. 16, no. 6, pp. 2943–2953, 2018, doi: 10.12928/TELKOMNIKA.v16i6.10148.
- [6] M. M. Uamusse, K. Tussupova, K. M. Persson, and R. Berndtsson, "Mini-grid hydropower for rural electrification in mozambique: Meeting local needs with supply in a nexus approach," *Water (Switzerland)*, vol. 11, no. 2, p. 305, 2019, doi: 10.3390/w11020305.
- [7] W. Ali, H. Farooq, A. Rasool, I. A. Sajjad, C. Zhenhua, and L. Ning, "Modeling and analysis of the dynamic response of an off-grid synchronous generator driven micro hydro power system," *Int. J. Renew. Energy Dev.*, vol. 10, no. 2, pp. 373–384, 2021, doi: 10.14710/ijred.2021.33567.
- [8] R. Sebastian C and P. P. Rajeevan, "A load commutated multilevel current source inverter fed open-end winding induction motor drive with regeneration capability," *IEEE Trans. Power Electron.*, vol. 35, no. 1, pp. 816–825, 2020, doi: 10.1109/TPEL.2019.2916224.
- [9] S. Shanmugasundaram, "Solar based Z source inverter for high power application," *Bull. Electr. Eng. Informatics*, vol. 6, no. 4, pp. 343–347, 2017, doi: 10.11591/eei.v6i4.863.
- [10] A. Belila, E. M. Berkouk, M. Benbouzid, Y. Amirat, B. Tabbache, and A. Mamoune, "Control methodology and implementation of a Z-source inverter for a stand-alone photovoltaic-diesel generator-energy storage system microgrid," *Electr. Power Syst. Res.*, vol. 185, p. 106385, 2020, doi: 10.1016/j.epsr.2020.106385.
- [11] M. Prasada, A. K. Akella, and A. Y. Abdelaziz, "Design and analysis of solar photovoltaic-fed Z-source inverter-based dynamic voltage restorer," *Sci. Iran.*, vol. 27, no. 6 D, pp. 3190–3203, 2020, doi: 10.24200/SCI.2019.51096.2000.
- [12] D. Sankar and C. A. Babu, "Design and analysis of impedance source based asymmetric inverter for PV application," *Int. J. Eng. Adv. Technol.*, vol. 9, no. 1, pp. 1593–1599, 2019, doi: 10.35940/ijeat.F8693.109119.
- [13] D. Sankar and C. A. Babu, "Design and analysis of a novel quasi Z source based asymmetric multilevel inverter for PV applications," *Int. J. Power Electron. Drive Syst.*, vol. 11, no. 3, pp. 1368–1378, 2020, doi: 10.11591/ijpeds.v11.i3.pp1368-1378.
- [14] S. Sonar, "A new configuration of three-level ZSI using transistor clamped topology," *Energies*, vol. 13, no. 6, p. 1469, 2020, doi: 10.3390/en13061469.
- [15] D. Chinmay V and D. Chaitanya V, "Optimum design of dynamic voltage restorer for voltage sag mitigation in distribution network," *Int. J. Power Electron. Drive Syst.*, vol. 10, no. 3, pp. 1364–1372, 2019, doi: 10.11591/ijpeds.v10.i3.1364-1372.
- [16] D. Mande, J. P. Trovão, and M. C. Ta, "Comprehensive review on main topologies of impedance source inverter used in electric vehicle applications," *World Electr. Veh. J.*, vol. 11, no. 2, p. 37, 2020, doi: 10.3390/WEVJ11020037.
- [17] E. Rajendran, D. C. Kumar, and D. P. Suresh, "Intensification of Power Quality Using PMSG and Cascaded Multi Cell Trans-Z-Source Inverter," *Circuits Syst.*, vol. 7, no. 11, pp. 3778–3793, 2016, doi: 10.4236/cs.2016.711316.
- [18] Z. Rasin, M. F. Rahman, M. Azri, M. H. N. Talib, and A. Jidin, "Design and development of grid-connected quasi-z-source pv inverter," *Int. J. Power Electron. Drive Syst.*, vol. 9, no. 4, pp. 1989–2005, 2018, doi: 10.11591/ijpeds.v9.i4.pp1989-2005.
- [19] M. Steinbring, M. Pacas, and M. Alnajjar, "Emulation of a micro-hydro-turbine for stand-alone power plants with Z-Source inverter," *IECON Proc. (Industrial Electron. Conf.)*, pp. 5291–5296, 2012, doi: 10.1109/IECON.2012.6388964.
- [20] H. A. Mosalam, R. A. Amer, and G. A. Morsy, "Fuzzy logic control for a grid-connected PV array through Z-source-inverter using maximum constant boost control method," *Ain Shams Eng. J.*, vol. 9, no. 4, pp. 2931–2941, 2018, doi: 10.1016/j.asej.2018.10.001.
- [21] N. Saeed, A. Ibrar, and A. Saeed, "A Review on Industrial Applications of Z-Source Inverter," *J. Power Energy Eng.*, vol. 5, no. 9, pp. 14–31, 2017, doi: 10.4236/jpee.2017.59002.
- [22] M. Teimoori, S. H. Edjtahed, and A. H. Niasar, "Design and Simulation of Z-Source Inverter Fed Brushless DC Motor Drive Supplied With Fuel Cell for Automotive Applications," *J. Power Electron. Power Syst.*, vol. 6, no. 3, pp. 60–71, 2016.
- [23] M. M. Roomi, "An Overview of Carrier-based Modulation Methods for Z-Source Inverter," *Power Electron. Drives*, vol. 4, no. 1, pp. 15–31, 2019, doi: 10.2478/pead-2019-0007.
- [24] R. Alla and A. Chowdhury, "Performance analysis of implanted hybrid three quasi Z source inverter designed for renewable energy conversion applications," *Electrica*, vol. 21, no. 1, pp. 1–9, 2021, doi: 10.5152/ELECTRICA.2020.19068.
- [25] S. Stepenko, O. Husev, D. Vinnikov, C. Roncero-Clemente, S. Pires Pimentel, and E. Santasheva, "Experimental Comparison of Two-Level Full-SiC and Three-Level Si-SiC Quasi-Z-Source Inverters for PV Applications," *Energies*, vol. 12, no. 13, p. 2509, Jun. 2019, doi: 10.3390/en12132509.
- [26] M. K. Nguyen and Y. O. Choi, "PWM control scheme for quasi-switched-boost inverter to improve modulation index," *IEEE Trans. Power Electron.*, vol. 33, no. 5, pp. 4037–4044, 2018, doi: 10.1109/TPEL.2017.2717487.
- [27] M. Siddique, A. Mubasher, R. F. Ahmad, K. Riaz, and N. Zahoor, "An Advanced Boost for Controlling the Gain and Minimizing the VS for ASC / SL-qZSI," *Pakistan J. Eng. Technol. PakJET*, vol. 4, no. 1, pp. 52–59, 2021.
- [28] N. M. Badrul Sham, S. Aizam Zulkifli, and R. Jackson, "i-Capacitor Voltage Control for PV Z-source System with Enhanced Shoot-through," *Int. J. Power Electron. Drive Syst.*, vol. 9, no. 4, p. 1899, 2018, doi: 10.11591/ijpeds.v9.i4.pp1899-1911.
- [29] H. Fathi and H. Madadi, "Enhanced-Boost Z-Source Inverters with Switched Z-Impedance," *IEEE Trans. Ind. Electron.*, vol. 63, no. 2, pp. 691–703, 2016, doi: 10.1109/TIE.2015.2477346.
- [30] X. Zhu, B. Zhang, and D. Qiu, "A New Nonisolated Quasi-Z-Source Inverter with High Voltage Gain," *IEEE J. Emerg. Sel. Top. Power Electron.*, vol. 7, no. 3, pp. 2012–2028, 2019, doi: 10.1109/JESTPE.2018.2873805.
- [31] B. S. Gadalla, E. Schaltz, Y. Siwakoti, and F. Blaabjerg, "Analysis of loss distribution of Conventional Boost, Z-source and Y-source Converters for wide power and voltage range," *Trans. Environ. Electr. Eng.*, vol. 2, no. 1, p. 1, Jan. 2017, doi: 10.22149/tee.v2i1.68.
- [32] J. N. Barath, A. Soundarrajan, S. Stepenko, O. Husev, D. Vinnikov, and M. K. Nguyen, "Topological review of quasi-switched boost inverters," *Electron.*, vol. 10, no. 12, p. 1485, 2021, doi: 10.3390/electronics10121485.
- [33] S. A. Zulkifli, M. R. Sewang, S. Salimin, and N. M. B. Shah, "Voltage control in Z-source inverter using low cost microcontroller for undergraduate approach," in *AIP Conference Proceedings*, 2017, vol. 1883, p. 020044, doi: 10.1063/1.5002062.
- [34] R. Palanisamy and K. Vijayakumar, "Maximum boost control for 7-level Z-source cascaded H-bridge inverter," *Int. J. Power Electron. Drive Syst.*, vol. 8, no. 2, pp. 739–746, 2017, doi: 10.11591/ijpeds.v8.i2.pp739-746.
- [35] N. Sabeur, S. Mekhilef, and A. Masaoud, "Extended maximum boost control scheme based on single-phase modulator for three-phase z-source inverter," *IET Power Electron.*, vol. 9, no. 4, pp. 669–679, 2016, doi: 10.1049/iet-pel.2015.0124.
- [36] M. Savio and S. Murugesan, "Harmonic evaluation of Z-source PWM inverter for wind powered industrial drive applications," *Int. J. Electr. Eng. Informatics*, vol. 6, no. 1, pp. 129–143, 2014, doi: 10.15676/ije.2014.6.1.9.
- [37] M. A. Mawlikar, "Design and Implementation of Z-source inverter using SBC," *Asian J. Conver. Technol.*, vol. 4, no. 2, pp. 1–8, 2018, doi: 10.33130/ASIAN.